PROCEEDINGS OF SCIENCE

TMD Evolution Effects on e^+e^- Annihilation Into Hadrons

Marco Radici*
Istituto Nazionale di Fisica Nucleare - Sezione di Pavia
via Bassi 6, I-27100 Pavia, Italy
E-mail: marco.radici@pv.infn.it

We calculate the transverse momentum dependence in the production of two back-to-back hadrons in electron-positron annihilations at the energy scales of BES-III and BELLE experiments, considering different combinations of pions and kaons. We use the parameters of the transverse-momentum-dependent (TMD) fragmentation functions that were recently extracted from the semi-inclusive deep-inelastic-scattering (SIDIS) multiplicities at low energy from HERMES . TMD evolution is applied according to different approaches and using different parameters for the nonperturbative part of the evolution kernel, thus exploring the sensitivity of our results to the partonic transverse momentum of intrinsic and radiative origin, and to its mixing with flavor. We discuss how experimental measurements could discriminate among the various scenarios.

QCD Evolution 2015 -QCDEV2015-
26-30 May 2015
Jefferson Lab (JLAB), Newport News Virginia, USA

*Speaker.

PoS(QCDEV2015)043

1. Introduction

Transverse momentum dependent (TMD) parton distribution functions (PDFs) and fragmentation functions (FFs) depend on the longitudinal and transverse components of the momentum of partons with respect to the parent hadron momentum, as well as on their flavor and polarization state. The TMD PDFs and TMD FFs enlarge the view established with ordinary integrated PDFs and FFs by exploring the multi-dimensional partonic structure of hadrons in momentum space. Several data for single- and double-spin asymmetries in semi-inclusive deep-inelastic scattering (SIDIS) can be interpreted as originating from the effect of specific combinations of (polarized) TMD PDFs and TMD FFs (see, e.g., Ref. [1]). The SIDIS process is useful because it gives simultaneous access to TMD PDFs and TMD FFs. But the factorized cross section always involves a convolution of initial and fragmenting parton transverse momenta: anticorrelation hinders a separate investigation of the two intrinsic distributions.

Therefore, we consider the semi-inclusive production of two back-to-back hadrons in electron-positron annihilations. In analogy with the SIDIS process, we define the multiplicities as the differential number of back-to-back pairs of hadrons produced per corresponding single-hadron production. Then, we study their transverse momentum distribution at large values of the center-of-mass (cm) energy, starting from an input expression for TMD FFs taken from the analysis of HERMES SIDIS multiplicities at low energy performed in Ref. [2]. In this framework, we can extract clean and uncontaminated details on the transverse-momentum dependence of the unpolarized TMD FF, which is a fundamental ingredient of any spin asymmetry in SIDIS and, therefore, it affects the extraction also of polarized TMD distributions.

The hard scales involved in e^+e^- annihilations are much larger than the average values explored in SIDIS by HERMES , which is assumed as the starting reference scale. To account for this scale dependence, the TMD functions must obey evolution equations that generalize the standard Renormalization Group Evolution (RGE) to a multi-scale regime in hard processes. TMD evolution equations have been derived for unpolarized TMD PDFs and TMD FFs [3, 4]. But the phenomenological implementation of these effects is still under active debate [5], and only recently an attempt of giving a (not complete) description was released [6].

Because of the wide range spanned between the typical SIDIS and e^+e^- scales, we can make realistic tests on the sensitivity to various implementations of TMD evolution available in the literature [7]. Moreover, in the analysis of HERMES SIDIS multiplicities a clear indication was found that different quark flavors produce different transverse-momentum distributions of final hadrons, although the flavor-independent fit of the data was not statistically excluded [2]. Here, we investigate also to which extent the annihilation rate is modified according to the flavor configurations of partonic transverse momenta, by considering different combinations of final pions and kaons [7].

2. Multiplicities for e^+e^-

We consider the process $e^+e^- \to h_1 h_2 X$ (see Fig. 1), where an electron e^- and a positron e^+ annihilate producing a virtual photon with time-like momentum transfer $q^2 \equiv Q^2 \geq 0$. The virtual photon emits a quark and an antiquark, which further fragment in two back-to-back jets. Each jet contains an unpolarized leading hadron: the hadron h_1 with momentum and mass P_1, M_1, in one

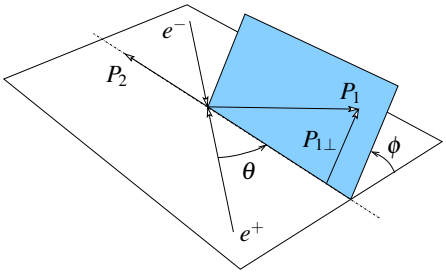

Figure 1: Kinematics for the e^+e^- annihilation leading to back-to-back hadrons with momenta P_1 and P_2.

emisphere, and the hadron h_2 with momentum and mass P_2, M_2 in the opposite emisphere. The fractional energies carried by the two hadrons are defined through the following invariants:

$$z_1 = \frac{2P_1\cdot q}{Q^2} \approx \frac{P_1\cdot P_2}{q\cdot P_2} \qquad z_2 = \frac{2P_2\cdot q}{Q^2} \approx \frac{P_2\cdot P_1}{q\cdot P_1}\,, \tag{2.1}$$

and we define also the invariant $y = P_2\cdot\ell/P_2\cdot q$, where ℓ is the electron momentum.

In the electron-positron cm frame, we select the frame where (q, P_2) have no transverse components; we choose $\hat{\boldsymbol{z}} = -\boldsymbol{P}_2$ and $P_1^\mu = (0, |\boldsymbol{P}_{1\perp}|\cos\phi, |\boldsymbol{P}_{1\perp}|\sin\phi, 0)$ (see Fig. 1). In the plane perpendicular to (P_1, P_2), $\boldsymbol{q}_T \neq 0$ and it holds $\boldsymbol{q}_T = -\boldsymbol{P}_{1\perp}/z_1$ up to corrections of order $1/Q^2$ [7]. We define also the angle $\theta = \arccos(\boldsymbol{\ell}\cdot\hat{\boldsymbol{z}}/|\boldsymbol{\ell}|)$ which is related to the invariant $y \approx (1+\cos\theta)/2$.

We consider a kinematics where $q_T^2 \ll Q^2$ and $M^2 \ll Q^2$. Hence, contributions to the cross section from perturbative terms at large transverse momenta or from higher twists are neglected. Moreover, the soft gluon radiation is here resummed at the Next-to-Leading-Log level (NLL), and the hard annihilation is calculated at leading order (LO) in α_S [7]. Then, the cross section for the e^+e^- annihilation into back-to-back pairs of unpolarized hadrons simplifies to

$$\frac{d\sigma^{h_1h_2}}{dz_1\,dz_2\,dq_T^2\,dy} \approx \frac{6\pi\alpha^2}{Q^2}\left(\frac{1}{2}-y+y^2\right)\sum_q e_q^2\int_0^\infty db_T\,b_T\,J_0(q_Tb_T)$$
$$\times\left[z_1^2 D_1^{q\to h_1}(z_1,b_T;\zeta_1,\mu)\,z_2^2 D_1^{\bar q\to h_2}(z_2,b_T;\zeta_2,\mu)+(q\leftrightarrow\bar q)\right], \tag{2.2}$$

where $q_T \equiv |\boldsymbol{q}_T|$ and $D_1^{q\to h}(z,b_T;\zeta,\mu)$ is the TMD FF in impact parameter space for an unpolarized quark with flavor q fragmenting into an unpolarized hadron h and carrying light-cone momentum fraction z and transverse momentum conjugated to b_T [8]. The TMD FF can be factorized at the renormalization/factorization scale μ and evolves with it through standard RGE. The $D_1^{q\to h}$ depends also on the scale ζ (with $\zeta_1\zeta_2 = Q^4$) which is connected to a rapidity cutoff necessary to isolate and define the TMD FF itself [3, 4]; we name ζ the rapidity scale.

In strict analogy with the SIDIS definition [9], we construct the e^+e^- multiplicities as the differential number of back-to-back pairs of hadrons produced per corresponding single-hadron production after the e^+e^- annihilation. In terms of cross sections, we have

$$M^{h_1h_2}(z_1,z_2,q_T^2,y) = \frac{d\sigma^{h_1h_2}}{dz_1\,dz_2\,dq_T^2\,dy}\Big/\frac{d\sigma^{h_1}}{dz_1\,dy}\,, \tag{2.3}$$

where $d\sigma^{h_1h_2}$ is the differential cross section of Eq. (2.2). The $d\sigma^{h_1}$ describes the production of a single hadron h_1 from the e^+e^- annihilation [10].

3. TMD evolution

We now address the evolution of the TMD FF with the factorization scale μ and the rapidity scale ζ. Different scenarios are possible according to the choice of the starting value for μ.

3.1 The μ_b prescription

The functional form of TMD FFs at small b_T can be calculated in perturbative QCD. Hence, it is convenient to introduce the new variable $\hat{b}_T$ that freezes at $b_{\rm max}$ when b_T becomes large. Consistently with the approximations leading to the cross section (2.2) and using the technique of Operator Product Expansion (OPE), the b_T–spectrum of TMD FFs can be described as [7]

$$\begin{aligned} D^{a\to h}(z,b_T;Q) &= e^{S_{\rm pert}(\hat{b}_T;Q,\mu_{\hat{b}})}\, e^{-g_{\rm np}(b_T)\log\frac{Q^2}{Q_0^2}}\, d_1^{a\to h}(z;\mu_{\hat{b}})\,\frac{1}{z^2}\, e^{-\frac{\langle \boldsymbol{P}_\perp^2\rangle^{a\to h}(z)}{4z^2}\,b_T^2} \\ &= R(b_T;Q,\mu_{\hat{b}},Q_0)\, D^{a\to h}(z,b_T;\mu_{\hat{b}})\,, \end{aligned} \tag{3.1}$$

where the collinear fragmentation function $d_1^{j\to h}$ for flavor j is evaluated at the running scale $\mu_{\hat{b}} = 2e^{-\gamma_E}/\hat{b}_T$ with γ_E the Euler constant. The Sudakov term $S_{\rm pert}$ describes the evolution with the factorization scale $\mu \equiv Q$ (starting from the scale $\mu_{\hat{b}}$ running with b_T) and the perturbative part at $\hat{b}_T \le b_{\rm max}$ of the evolution with ζ (starting again from the running $\mu_{\hat{b}}^2$). The model-dependent function $g_{\rm np}$ describes the nonperturbative part at large b_T of the evolution with ζ starting from the scale Q_0^2. At this initial scale, the input transverse-momentum dependence of TMD FFs is represented in configuration space by the shown Gaussian ansatz, where $\langle \boldsymbol{P}_\perp^2\rangle^{a\to h}(z)$ is the flavor- and z-dependent Gaussian width. This form is suggested by the analysis performed in Ref. [2] of the transverse-momentum dependence of SIDIS multiplicities measured by HERMES [9].

Hence, the net effect of TMD evolution can be represented as the action of an operator R on the input TMD FF evaluated at the scale $\mu_{\hat{b}}$, which is running with b_T. This peculiar feature grants that there is a smooth matching between the perturbative domain at small b_T and the nonperturbative domain at large b_T. However, it does not allow to unambiguously recover the initial TMD FF when switching off evolution effects. In fact, for $Q = \mu_{\hat{b}}$ the R operator does not become the identity because $\mu_{\hat{b}} \neq Q_0$. In practice, if Q_0 is identified with the average scale of the HERMES data for SIDIS multiplicities [9], namely $Q_0^2 = 2.4\ {\rm GeV}^2$, it is easy to find a value of $b_{\rm max}$ such that $\mu_{\hat{b}} \approx Q_0$, because the HERMES kinematics overlaps with the domain of large b_T where $\hat{b}_T \approx b_{\rm max}$ [7].

Following Refs. [11, 12], we choose $g_{\rm np}$ to be

$$g_{\rm np}^{\rm lin}(b_T) = \frac{g_2}{4}\, b_T^2\,, \quad \text{or} \quad g_{\rm np}^{\rm log}(b_T) = g_2\, \bar{b}_T^2\, \ln\left(1+\frac{b_T^2}{4\bar{b}_T^2}\right), \quad \bar{b}_T = 1\ {\rm GeV}^{-1}\,, \tag{3.2}$$

where $b_{\rm max}$ and g_2 are anticorrelated [7]. We choose values inspired to Refs. [11, 12].

We also explored different expressions for $\hat{b}_T$:

$$\hat{b}_T \equiv b_T^* = \frac{b_T}{\sqrt{1+\frac{b_T^2}{b_{\rm max}^2}}}\,, \quad \hat{b}_T \equiv b_T^\dagger = b_{\rm max}\left\{1-\exp\left[-\frac{b_T^4}{b_{\rm max}^4}\right]\right\}^{\frac{1}{4}}. \tag{3.3}$$

The first one is the socalled "b-star" prescription [3, 11]; the second one approaches the asymptotic constant $b_{\rm max}$ more steeply and quickly.

In principle, we have four different combinations of prescriptions. However, some of them produce redundant results and have been neglected. In summary, the transverse-momentum spectrum of the multiplicities in Eq. (2.3) has been analyzed by varying the anticorrelated pair of parameters $\{b_{\rm max}, g_2\}$, and by considering only the two combinations $\{b_T^*, g_{\rm np}^{\rm lin}\}$ and $\{b_T^\dagger, g_{\rm np}^{\rm log}\}$.

3.2 The fixed-scale prescription

We can write the evolution of TMD FFs in an alternative way to Eq. (3.1) by fixing the initial scale at the value $Q_i^2 \equiv Q_0^2 = 2.4$ GeV^2 for the whole b_T distribution. With this choice, it is not possible to apply OPE for calculating a perturbative tail to which the TMD FF should match at low b_T: we need a model input over the whole b_T spectrum. In our case, it is natural to identify the input TMD FF at the starting scale Q_i with the Gaussian parametrization of Eq. (3.1) equipped with the collinear d_1 evaluated at Q_0. Then, the expression for the evolved TMD FF becomes [7]

$$D^{a\to h}(z,b_T;Q) = e^{S_{\rm pert}(b_T;Q,Q_i)}\, d_1^{a\to h}(z;Q_i)\, \frac{1}{z^2}\, e^{-\frac{\langle \boldsymbol{P}_\perp^2\rangle^{a\to h}(z)}{4z^2} b_T^2}\,. \tag{3.4}$$

The nonperturbative Sudakov term involving $g_{\rm np}$ is included in $S_{\rm pert}$, which is valid for all the b_T spectrum. It actually accounts for the nonperturbative part of the evolution with ζ from $\mu_{\hat{b}}$ to Q_i [7].

4. Results for TMD multiplicities

The flavor sum in Eq. (2.2) can be simplified using the symmetry of TMD FFs upon charge-conjugation transformations, and distinguishing *favored* from *unfavored* fragmentation [7]. The flavor- and z-dependence of the Gaussian ansatz in Eq. (3.1) is described in total by seven fitting parameters [2]. For the collinear functions $d_1^{q\to h}(z;Q_0^2)$, we adopt the parametrization of Ref. [13]. Results are presented as normalized multiplicities $M^{h_1h_2}(z_1,z_2,q_T^2,y)/M^{h_1h_2}(z_1,z_2,0,y)$ for the hadron pair (h_1,h_2), where M is defined in Eq. (2.3). In such way, we are able to directly compare the genuine trend in q_T^2 for each different case. If not explicitly specified, we choose $y = 0.2$. For each specific case, the results are displayed as uncertainty bands: they represent the 68% of the envelope of 200 different curves produced from 200 different values for the vector of seven intrinsic parameters describing the Gaussian ansatz in Eq. (3.1). They are obtained by fitting the SIDIS multiplicities measured by the HERMES collaboration [9] (see Ref. [2]).

We first explore the sensitivity of our predictions to different values of the pair $b_{\rm max}$ [GeV^{-1}] and g_2 [GeV^2] (hereafter, we omit their units for simplicity). In Fig. 2, the normalized multiplicity for a $(\pi^+\pi^-)$ pair with $z_1 = z_2 = 0.5$ is shown as a function of $\boldsymbol{P}_{hT}^2 \equiv \boldsymbol{P}_{1\perp}^2 = z_1^2 \boldsymbol{q}_T^2$ at the BELLE scale $Q^2 = 100$ GeV^2 for the μ_b evolution scheme and with the $\{b_T^*, g_{\rm np}^{\rm lin}\}$ prescription for the transition to the nonperturbative regime. The uncertainty bands correspond to $\{b_{\rm max} = 1.5, g_2 = 0.18\}$ (dot-dashed borders), $\{b_{\rm max} = 1, g_2 = 0.43\}$ (dashed borders), $\{b_{\rm max} = 0.5, g_2 = 0.68\}$ (solid borders). The squared box with error bar indicates a hypothetical experimental error of 7%. It seems small enough to discriminate among the different predictions. Two additional light-gray bands are shown, which are partially overlapped (dot-dashed borders) or completely overlapped (dashed borders) to the band with solid borders. These bands reproduce the outcome of calculations performed in the same conditions but for $\mu_b/2$ (dot-dashed borders) and $2\mu_b$ (dashed borders). The almost complete

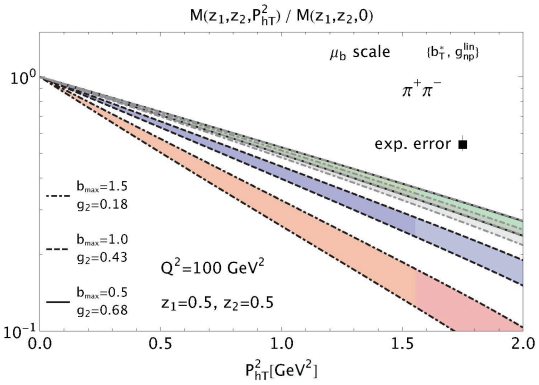

Figure 2: The normalized multiplicity for a $(\pi^+\pi^-)$ pair with $z_1 = z_2 = 0.5$ as a function of $\boldsymbol{P}_{hT}^2 \equiv \boldsymbol{P}_{1\perp}^2 = z_1^2 \boldsymbol{q}_T^2$ at the BELLE scale $Q^2 = 100$ GeV^2 for the μ_b evolution scheme and with the $\{b_T^*, g_{\rm np}^{\rm lin}\}$ prescription for the transition to the nonperturbative regime (see text). The uncertainty bands correspond to $\{b_{\rm max} = 1.5, g_2 = 0.18\}$ (dot-dashed borders), $\{b_{\rm max} = 1, g_2 = 0.43\}$ (dashed borders), $\{b_{\rm max} = 0.5, g_2 = 0.68\}$ (solid borders). The latter is accompanied by light-gray bands for results with the same parameters but with the choice $\mu_b/2$ (dot-dashed borders) or $2\mu_b$ (dashed borders). An experimental error of 7% is also indicated.

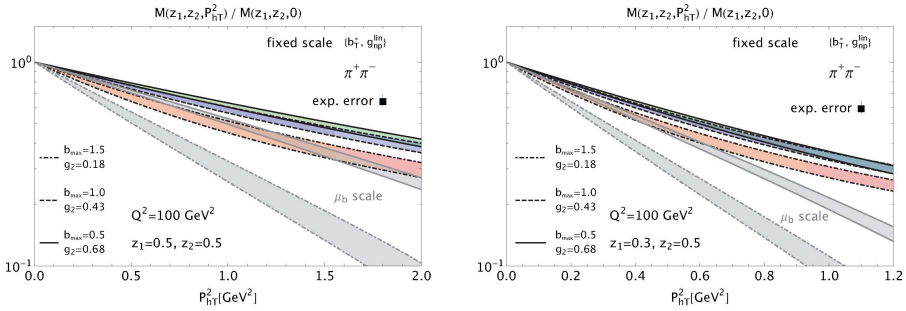

Figure 3: The normalized multiplicity for a $(\pi^+\pi^-)$ pair as a function of $\boldsymbol{P}_{hT}^2 \equiv \boldsymbol{P}_{1\perp}^2 = z_1^2 \boldsymbol{q}_T^2$ in the same conditions and with the same notation as in Fig. 2 but for the "fixed-scale" evolution scheme. Left panel for $z_1 = z_2 = 0.5$, right panel for $z_1 = 0.3, z_2 = 0.5$. The additional light-gray bands with dot-dashed and solid borders are the result related to the "μ_b" evolution scheme for $\{b_{\rm max} = 1.5, g_2 = 0.18\}$ and $\{b_{\rm max} = 0.5, g_2 = 0.68\}$, respectively.

overlap of these results shows that for the selected observable the sensitivity to the arbitrary choice of the matching scale μ_b is negligible.

Next, we explore the sensitivity of the normalized multiplicity to the choice of the evolution scheme. In Fig. 3, the normalized multiplicity for a $(\pi^+\pi^-)$ pair is shown as a function of $\boldsymbol{P}_{hT}^2 \equiv \boldsymbol{P}_{1\perp}^2 = z_1^2 \boldsymbol{q}_T^2$ in the same conditions and with the same notation as in Fig. 2 but for the "fixed-scale" evolution scheme. The left panel displays pion pairs with $z_1 = z_2 = 0.5$, the right panel with $z_1 = 0.3, z_2 = 0.5$. The two additional light-gray bands correspond to the results with the "μ_b" evolution scheme for $\{b_{\rm max} = 1.5, g_2 = 0.18\}$ (dot-dashed borders) and $\{b_{\rm max} = 0.5, g_2 = 0.68\}$ (solid borders). In the left panel, it is important to notice that there is a significant overlap between the "fixed-scale" band with maximum $b_{\rm max}$ (dot-dashed borders) and the "μ_b" light-gray band with minimum $b_{\rm max}$ (solid borders). Apparently, the normalized multiplicity seems not enough sensitive

to discriminate among different evolution schemes. However, this result is observed at $z_1 = z_2 = 0.5$. In the right panel, the same situation is reproduced with $z_1 = 0.3$ and $z_2 = 0.5$. Now, the two bands are well separated and can be distinguished by the indicated hypothetical experimental error around 7%. Therefore, only when combining the study of both the z and $\boldsymbol{P}_{1\perp}^2$ dependencies in the normalized multiplicity we may be able to discriminate among different TMD evolution schemes.

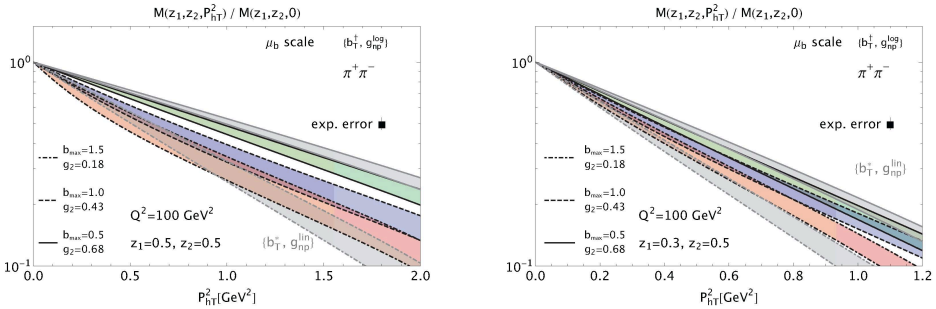

Figure 4: The normalized multiplicity for a $(\pi^+\pi^-)$ pair at $z_2 = 0.5$ as a function of $\boldsymbol{P}_{hT}^2 \equiv \boldsymbol{P}_{1\perp}^2 = z_1^2 \boldsymbol{q}_T^2$ at the BELLE scale $Q^2 = 100$ GeV^2 for the "μ_b" evolution scheme and with the $\{b_T^\dagger, g_{\rm np}^{\rm log}\}$ prescription for the transition to the nonperturbative regime (see text). Notation for the uncertainty bands as in previous figure. The additional light-gray bands with dot-dashed and solid borders are the result with the $\{b_T^*, g_{\rm np}^{\rm lin}\}$ matching prescription for $\{b_{\rm max} = 1.5, g_2 = 0.18\}$ and $\{b_{\rm max} = 0.5, g_2 = 0.68\}$, respectively. Left panel for $z_1 = 0.5$, right panel for $z_1 = 0.3$.

We now consider the possibility of discriminating among the two different functional dependences for $g_{\rm np}(b_T)$ in Eq. (3.2), or among the two prescriptions for $\hat{b}_T(b_T)$ in Eq. (3.3). In Fig. 4, the normalized multiplicity for a $(\pi^+\pi^-)$ pair is shown as a function of $\boldsymbol{P}_{hT}^2 \equiv \boldsymbol{P}_{1\perp}^2 = z_1^2 \boldsymbol{q}_T^2$ at the BELLE scale $Q^2 = 100$ GeV^2 for the "μ_b" evolution scheme. A group of uncertainty bands displays the results for the $\{b_T^\dagger, g_{\rm np}^{\rm log}\}$ prescription in the standard notation, *i.e.* for $\{b_{\rm max} = 1.5, g_2 = 0.18\}$ (dot-dashed borders), $\{b_{\rm max} = 1, g_2 = 0.43\}$ (dashed borders), and $\{b_{\rm max} = 0.5, g_2 = 0.68\}$ (solid borders). The two light-gray bands correspond to the results with the $\{b_T^*, g_{\rm np}^{\rm lin}\}$ prescription for $\{b_{\rm max} = 1.5, g_2 = 0.18\}$ (dot-dashed borders) and $\{b_{\rm max} = 0.5, g_2 = 0.68\}$ (solid borders). In the left panel where $z_1 = z_2 = 0.5$, the two bands with dot-dashed borders are substantially overlapped, suggesting that it might not be possible to discriminate between the $\{b_T^*, g_{\rm np}^{\rm lin}\}$ and $\{b_T^\dagger, g_{\rm np}^{\rm log}\}$ prescriptions. In the right panel, the same calculation is performed at $z_1 = 0.3$, $z_2 = 0.5$, and a sufficiently small experimental error could discriminate between the two bands. Unfortunately, the plot suggests also that this option seems possible only for the $\{b_{\rm max} = 1.5, g_2 = 0.18\}$ case. And further explorations show that the same calculation, when performed in the "fixed-scale" evolution scheme, produces more confused results.

In summary, we find that only the combined study of the z and $\boldsymbol{P}_{1\perp}^2$ dependencies of the normalized multiplicity allows for discerning results obtained from different parametrizations and prescriptions in the description of nonperturbative effects in the TMD evolution. This is not accidental. The main difference between the two considered evolution schemes lies in fact in the z dependence of the collinear fragmentation function d_1, as it can be deduced by comparing Eqs. (3.1) and (3.4).

Previous results have been obtained at the BELLE scale of $Q^2 = 100$ GeV^2. In Fig. 5, the normalized multiplicity for a $(\pi^+\pi^-)$ pair at $z_1 = z_2 = 0.5$ is shown as a function of $\boldsymbol{P}_{hT}^2 \equiv \boldsymbol{P}_{1\perp}^2 =$

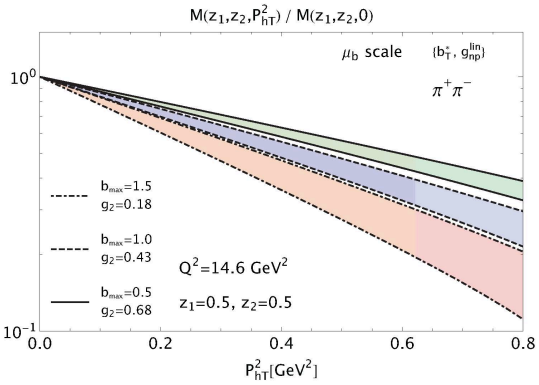

Figure 5: The normalized multiplicity for a $(\pi^+\pi^-)$ pair at $z_1 = z_2 = 0.5$ as a function of $\boldsymbol{P}_{hT}^2 \equiv \boldsymbol{P}_{1\perp}^2 = z_1^2 \boldsymbol{q}_T^2$ at the BES-III scale $Q^2 = 14.6\ \text{GeV}^2$ for the "μ_b" evolution scheme and with the $\{b_T^*, g_{\rm np}^{\rm lin}\}$ prescription (see text). Notation and conventions for the uncertainty bands as in Fig. 2.

$z_1^2 \boldsymbol{q}_T^2$ in the same conditions and notation as in Fig. 2 but at the BES-III scale $Q^2 = 14.6\ \text{GeV}^2$. With respect to Fig. 2, we deduce that the net effect is a systematic enlargement of the uncertainty bands. This finding occurs also for other combinations of evolutions schemes and nonperturbative prescriptions. Hence, we deduce that working at the BES-III scale is not useful if we want to discriminate among different evolution parameters, prescriptions, or schemes. However, we recall that each uncertainty band is the envelope of the 68% of 200 different replicas. Then, we might envisage that a sufficiently small experimental error could discriminate some of them, in order to narrow the uncertainty on the intrinsic parameters of the Gaussian ansatz.

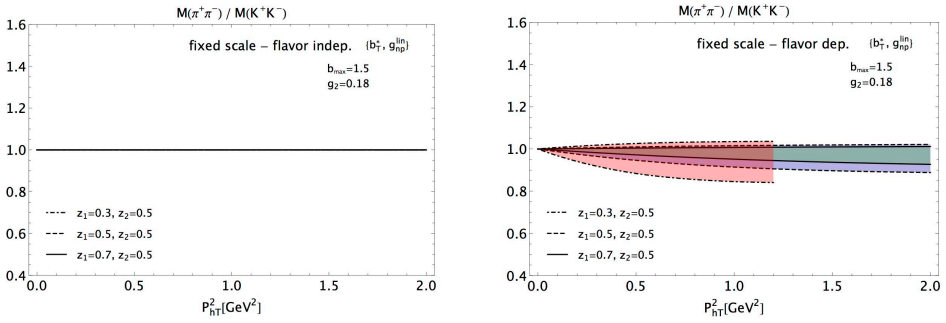

Figure 6: The ratio of normalized multiplicities between $\{\pi^+\pi^-\}$ and $\{K^+K^-\}$ final pairs at $z_2 = 0.5$ and $y = 0.2$ as a function of $\boldsymbol{P}_{hT}^2 \equiv \boldsymbol{P}_{1\perp}^2 = z_1^2 \boldsymbol{q}_T^2$ at the BELLE scale $Q^2 = 100\ \text{GeV}^2$ for the "fixed-scale" evolution scheme, for the evolution parameters $\{b_{\rm max} = 1.5, g_2 = 0.18\}$, and with the $\{b_T^*, g_{\rm np}^{\rm lin}\}$ prescription (see text). Uncertainty bands with dot-dashed, dashed, and solid borders for $z_1 = 0.3, 0.5, 0.7$, respectively. Left panel for flavor independent intrinsic parameters of input TMD FF, right panel for flavor dependent ones (see text).

The cross section in Eq. (2.2) mixes all flavors in the sum. Therefore, it is useful to define an observable that is well suited to explore the effect of flavor in the TMD evolution. We consider this observable to be the ratio of normalized multiplicities corresponding to different hadron species. In Fig. 6, the ratio of normalized multiplicities between $\{\pi^+\pi^-\}$ and $\{K^+K^-\}$ final pairs at $z_2 = 0.5$

and $y = 0.2$ is displayed as a function of $\boldsymbol{P}_{hT}^2 \equiv \boldsymbol{P}_{1\perp}^2 = z_1^2 \boldsymbol{q}_T^2$ at the BELLE scale $Q^2 = 100$ GeV^2 for the "fixed-scale" evolution scheme, for the evolution parameters $\{b_{\rm max} = 1.5, g_2 = 0.18\}$, and with the $\{b_T^*, g_{\rm np}^{\rm lin}\}$ prescription. If we suppose to switch off the flavor dependence of the intrinsic parameters, the b_T distribution of the TMD FF is controlled by the same Gaussian width $\langle \boldsymbol{P}_\perp^2 \rangle(z)$ for all channels. This feature remains valid when performing the Bessel transform to momentum space, such that the $\boldsymbol{q}_T^2$ distribution of the cross section can be factorized out of the flavor sum. Therefore, if we take the ratio of normalized multiplicities at the same z_1 we expect the latter to be independent of $\boldsymbol{P}_{1\perp}^2 = z_1^2 \boldsymbol{q}_T^2$. This is indeed the result displayed in the left panel of Fig. 6. It is a systematic feature of the "fixed-scale" evolution scheme: it holds true for other values of z_1 as well as for other combinations of nonperturbative evolution parameters and nonperturbative prescriptions. If we account for the flavor dependence of the Gaussian widths $\langle \boldsymbol{P}_\perp^2 \rangle^{q\to h}(z)$, then the b_T distribution is different for the $\{\pi^+\pi^-\}$ final state from the one for $\{K^+K^-\}$. Consequently, the ratio of normalized multiplicities has a specific $\boldsymbol{P}_{1\perp}^2 = z_1^2 \boldsymbol{q}_T^2$ distribution that, of course, changes with z_1. This is indeed the content of the right panel in Fig. 6: the uncertainty band of the 68% of 200 replicas of Gaussian widths with dot-dashed borders corresponds to $z_1 = 0.3$, the band with dashed borders to $z_1 = 0.5$, the band with solid borders to $z_1 = 0.7$. Almost all the ratios are smaller than unity because the $\boldsymbol{P}_{1\perp}^2$ distribution of the fragmentation into kaons seems to be larger than the corresponding one for pions [2]. In any case, the ratio of normalized multiplicities for different final hadrons is a useful tool to discriminate among different scenarios in TMD evolution. For example, if we change evolution scheme the behaviour of the ratio can be reversed.

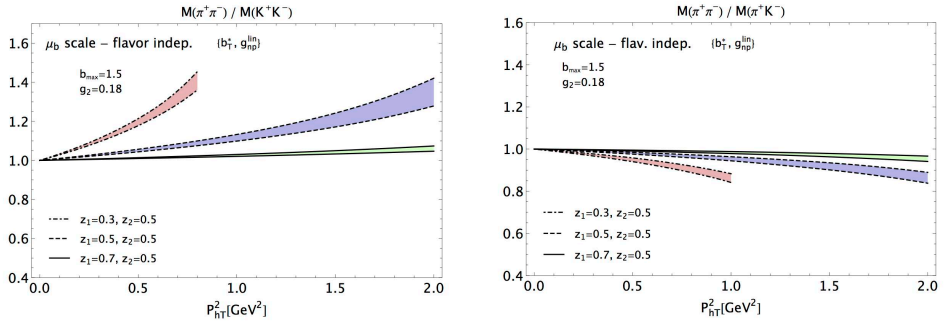

Figure 7: Left panel: same as in left panel of previous figure but for the "μ_b" evolution scheme. Right panel: the ratio between the normalized multiplicities of $\{\pi^+\pi^-\}$ and $\{\pi^+K^-\}$ final states in the same conditions and with the same notation as in the left panel.

In Fig. 7, the left panel shows the same ratio of normalized multiplicities in the same conditions and notation as in the left panel of the previous figure but for the "μ_b" evolution scheme. In this scheme, the b_T distribution of the TMD FF is influenced also by the collinear part of the fragmentation function: the $d_1^{q\to h}$ in Eq. (3.1) is evaluated at the running scale $\mu_{\hat{b}}$ which is related to b_T. Hence, when performing the Bessel transform of D_1^q in the cross section, the resulting $\boldsymbol{q}_T^2$ distribution depends on the flavor of the fragmenting parton even if the intrinsic parameters do not, as shown in the figure. Surprisingly, now all the ratios are larger than unity. When including also the flavor dependence in the intrinsic parameters, the two effects mix up and the uncertainty bands become larger [7]. in this case, we can argue that experimental data will have a sufficiently

small error to discriminate among the various replicas of the intrinsic parameters. The right panel of Fig. 7 displays the ratio between $\{\pi^+\pi^-\}$ and $\{\pi^+K^-\}$ final states in the same notation and conventions as in the left panel. All the ratios are now lower than unity. Hence, combining this result with the content of the left panel could represent a very selective test of the "μ_b" evolution scheme: the $\boldsymbol{P}_{1\perp}^2$ distribution of normalized multiplicities for the $\{\pi^+\pi^-\}$ final state should be larger than the one for $\{K^+K^-\}$ at any z_1, while at the same time it should turn out narrower than the one for $\{\pi^+K^-\}$ at any z_1.

Finally, because of charge conjugation symmetry we predict that the ratio between normalized multiplicities leading to (π^+, K^-) and (π^-, K^+) final states should be equal to unity, irrespective of the choice of evolution schemes, nonperturbative evolution parameters and prescriptions. It would be interesting to cross-check this prediction by measuring this ratio as a function of $\boldsymbol{P}_{1\perp}^2$.

References

[1] A. Bacchetta *et al.*, *Semi-inclusive deep inelastic scattering at small transverse momentum*, *JHEP* **02** (2007) 093 [hep-ph/0611265].

[2] A. Signori, A. Bacchetta, M. Radici, and G. Schnell, *Investigations into the flavor dependence of partonic transverse momentum*, *JHEP* **1311** (2013) 194 [arXiv:1309.3507 [hep-ph]].

[3] J. Collins, *Foundations of Perturbative QCD*, Cambridge University Press, Cambridge 2011.

[4] M.G. Echevarria, A. Idilbi, A. Schäfer, and I. Scimemi, *Model-Independent Evolution of Transverse Momentum Dependent Distribution Functions (TMDs) at NNLL*, *Eur. Phys. J.* **C73** (2013) 2636 [arXiv:1208.1281 [hep-ph]].

[5] R. Angeles-Martinez *et al.*, *Transverse momentum dependent (TMD) parton distribution functions: status and prospects*, arXiv:1507.05267 [hep-ph] (2015).

[6] Z.-B. Kang, A. Prokudin, P. Sung, and F. Yuan, *Extraction of Quark Transversity Distribution and Collins Fragmentation Functions with QCD Evolution* arXiv:1505.05589 [hep-ph] (2015).

[7] A. Bacchetta *et al.*, *Effects of TMD evolution and partonic flavor on e^+e^- annihilation into hadrons*, *JHEP* in press (2015) [arXiv:1508.00402 [hep-ph]].

[8] D. Boer, L. Gamberg, B. Musch, and A. Prokudin, *Bessel-Weighted Asymmetries in Semi Inclusive Deep Inelastic Scattering*, *JHEP* **1110** (2011) 021 [arXiv:1107.5294 [hep-ph]].

[9] A. Airapetian *et al.* (HERMES Coll.), *Multiplicities of charged pions and kaons from semi-inclusive deep-inelastic scattering by the proton and the deuteron*, *Phys. Rev. D* **87** (2013) 074029 [arXiv:1212.5407 [hep-ex]].

[10] D. Boer, R. Jakob, and P.J. Mulders, *Asymmetries in polarized hadron production in e+ e- annihilation up to order 1/Q*, *Nucl. Phys.* **B504** (1997) 345 [hep-ph/9702281].

[11] F. Landry, R. Brock, P.M. Nadolsky, and C.P. Yuan, *Tevatron Run-1 Z boson data and Collins-Soper-Sterman resummation formalism*, *Phys. Rev. D* **67** (2003) 073016 [hep-ph/0212159].

[12] A.V. Konychev and P.M. Nadolsky, *Universality of the Collins-Soper-Sterman nonperturbative function in gauge boson production*, *Phys. Lett.* **B633** (2006) 710 [hep-ph/0506225].

[13] D. de Florian, R. Sassot, and M. Stratmann, *Global analysis of fragmentation functions for pions and kaons and their uncertainties*, *Phys. Rev. D* **75** (2007) 114010 [hep-ph/0703242].